ChemPhysChem

Research Article
doi.org/10.1002/cphc.202200614

Chemistry Europe
European Chemical Societies Publishing

www.chemphyschem.org

Insight into the Interaction of Furfural with Metallic Surfaces in the Electrochemical Hydrogenation Process

Thorben Lenk[+],[a, b] Sahar Rabet[+],[b, c] Miriam Sprick,[b, c] Gabriele Raabe,*[b, c] and Uwe Schröder*[b, d]

Electrocatalytic hydrogenation of furfural on metal surfaces has become an important research subject due to the potential of the reaction product 2-methylfuran as a renewable energy resource. Identifying effective determinants in this reaction process requires a thorough investigation of the complex electrode-electrolyte interactions, which considers a variety of the influential components. In this work, *in operando* electrochemical Raman Spectroscopy and Molecular Dynamics simulations were utilized to investigate different characteristics of the interface layer in the electrocatalytic hydrogenation of furfural. Hereby, the influence of applied potentials, electrode material, and electrolyte composition were investigated in detail. The studied parameters give an insight into furfural's binding situation, molecular orientation, and reaction mechanism.

Introduction

The adverse effects of the exploitation of fossil resources on the world's climate are widely acknowledged, and consequently new sources for raw materials in chemical production and powering transportation must be found. Compounds obtained from biomass can be one of several solutions. Various chemicals extracted from biomass are suitable for utilization in modern industrial processes to satisfy society's resource needs. Furanic compounds, such as furfural (FF), can be obtained from cellulose biomass and subsequently be upgraded towards potential fuels and chemical production components.[1,2] 2-Methylfuran (MF) and furfuryl alcohol (FA) can be produced by hydrogenation of FF. While FA has potential applications in resin and polyether production, MF has been proposed as an electrofuel.[3,4] An electrochemical production of both chemicals as an alternative to a thermal catalytic reaction process has been frequently investigated in recent years. It has been shown that Cu electrodes in highly acidic media can produce mainly MF, whereas other electrode materials and more neutral pH values mainly yield FA and the radical coupling product hydrofuroin (HF).[5–9] Production of FA as a major product on Cu depends on the pH value in contrast to hydrofuroin, which is not formed. A. May et al. could show the rate-determining steps of the hydrogenation reaction mechanism towards MF and FA and suggest a Langmuir-Hinshelwood mechanism.[10] Figure 1 shows the different reaction products of electrochemical reductions of FF. Electrochemical reactions in aqueous media are in accordance with several of the 12 rules of green chemistry.[11] Combined with excess power from renewable energy sources, they can aid in storing overproduced electrical

[a] *T. Lenk*[+]
Institute of Environmental and Sustainable Chemistry, TU Braunschweig
Hagenring 30, 38106 Braunschweig, Germany
[b] *T. Lenk,*[+] *S. Rabet,*[+] *M. Sprick, Dr. G. Raabe, Prof. Dr. U. Schröder*
Cluster of Excellence SE[2]*A-Sustainable and Energy-Efficient Aviation,*
TU Braunschweig, Braunschweig, Germany
[c] *S. Rabet,*[+] *M. Sprick, Dr. G. Raabe*
Institute of Thermodynamics, TU Braunschweig
Hans-Sommer-Straße 5, 38106 Braunschweig, Germany
E-mail: G.Raabe@tu-braunschweig.de
Homepage: www.tu-braunschweig.de/en/ift/institute/divisions/group-molecular-thermodynamics
[d] *Prof. Dr. U. Schröder*
Institute for Biochemistry, University of Greifswald
Felix-Hausdorff-Straße 4, 17487 Greifswald, Germany
E-mail: Uwe.schroeder@uni-greifswald.de
Homepage: www.biochemie.uni-greifswald.de/en/forschung/forschung-in-den-arbeitskreisen/electrobiochemistry/
[+] *These authors contributed equally.*

Supporting information for this article is available on the WWW under https://doi.org/10.1002/cphc.202200614

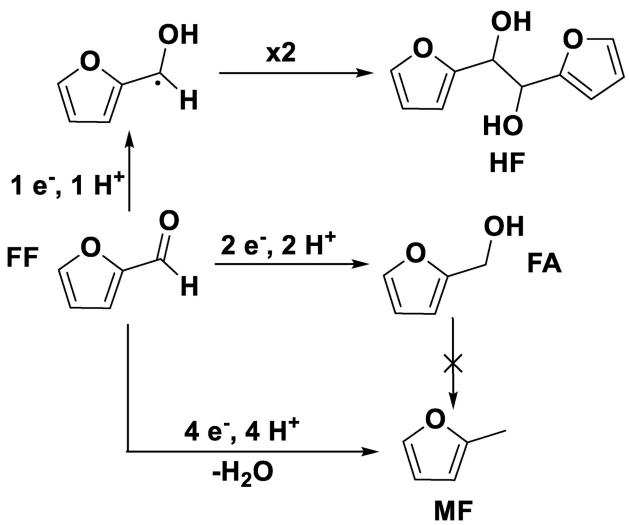

Figure 1. Schematic overview of reductive pathways from FF as starting material.

energy chemically and hence lower the carbon footprint for other applications, where a carbon-neutral solution can hardly be realized. A utilization as aviation fuel is one of the possible examples.

In the last decades, an increasing attentiveness was addressed towards electrochemical synthesis routes due to their multitude of advantages compared to conventional thermal reaction routes. At the same time, Raman spectroscopic methods have been developed and improved, leading to a variety of publications utilizing *in operando* electrochemical Raman spectroscopy[12] to receive a deeper insight into adsorption processes,[13] reaction intermediates[14] and the reaction mechanisms of electroorganic reactions.[15–17] Due to their potential role in future energy and resource management, electrohydrogenation reactions of furanic compounds were also investigated in spectroelectrochemical experiments. In this context, the group of N. Kornienko studied the electrochemical oxidation reaction of 5-hydroxymethylfurfural (HMF) on Au surfaces and transition metal oxides of Co, Fe, Ni, and respective mixtures deposited on Au.[15,16] J. Anibal et al. performed *in situ* ATR-SEIRAS (attenuated total reflection-surface-enhanced infrared absorption spectroscopy) of FF on Cu and Pb electrodes in pH 6.7 phosphate buffer medium.[18] They observed relatively weak electrode/molecule interactions on Cu, based on low deviations between bulk and surface vibration band wavenumbers and potential independence of the respective FF shifts. Furthermore, a surface concentration-dependent orientation was observed. While a more parallel FF orientation was observed for lower coverages, higher surface coverages led to a more perpendicular orientation to allow denser packing of FF molecules.[18] Finally, J. Li et al. gave an insight into the FF/electrode interaction during an electrochemical hydrogenation of FF on a copper electrode with sulfate electrolyte at pH 3.[19] Although several studies were conducted, Raman spectroscopic investigations using strongly acidic electrolyte conditions on Ag and Cu electrodes have not been performed so far. Though a direct comparison of different reaction conditions is required for an understanding of the electrochemical system.

Beside *in operando* electrochemical Raman spectroscopy, atomistic simulations are suitable methods to gain an insight into the behaviour of different components in an electrochemical cell. Quantum chemical simulations have already been used to study the hydrogenation reaction of furan family members. Wang et al.[20] used DFT (Density Functional Theory) ab-initio calculation to study the FF bonding configuration at Pd (111) interface and at water-Pd interface. They found that FF adsorbed on the metallic electrode in a way that the furan ring stays parallel to the surface. This observation, besides other calculations, concluded that the FF reaction at Pd (111) moves toward decarbonylation of the FF. Vorotnikov et al.[21] performed DFT calculations on FF, FA, MF, and furan on Pd (111). They showed that the preferable adsorption configuration for all components was the parallel furan ring to the surface. They also found that, in vacuum conditions, the thermodynamically favorable reaction path for FF on the Pd electrode is producing furan and CO. In another DFT investigation, Shi et al.[22] investigated the adsorption behavior of FF in the gas phase at Cu (111). They determined the most favorable reaction path and rate-determining step of FF conversion to FA and MF on a hydrogen-rich copper surface. They also found that FA and MF should be produced in quite the same quantity. In one study, Zhao et al.[23] investigated the hydrogenation of FF on water-Pd (111) interface with ab-initio MD calculations. They found that water affects the hydrogenation rate of FF in an electrocatalytic reaction by reducing the activation barrier energy.

Despite the accuracy of ab-initio methods for precisely modeling of the electronic structure, they are just applicable for small systems with few numbers of atoms and in a short duration due to the high computational cost.[24,25] On the other hand, molecular dynamics simulations (MD) based on classical force field can provide a compromise between accuracy and computational cost. Moreover, the new development in the MD methods to model constant potential electrodes and polarizability of metallic electrodes at the interface[26–28] make this method a suitable approach to study electrochemical cells.[24] However, to our best knowledge, there are no MD studies available on the reaction system of the furfural electrohydrogenation.

According to its potential importance in the future energy, transportation, and material markets, a deeper understanding of the mechanism of electrochemical reactions such as the electrohydrogenation and electrodeoxygenation reaction of FF is crucial for a further development of this technique. Due to the complexity of electrode-electrolyte interactions and various effective components in an electrochemical reaction, recognizing influential determinants for the systematic and optimized synthesis procedure has paramount importance. Previous works focused on isolated aspects or gained information from only one source of either experimental or simulational information, missing a combination of both to gain an even deeper understanding and support respective interpretations. Therefore, in this work both *in operando* electrochemical Raman spectroscopy and MD simulations are exploited to provide a deeper insight into the reaction mechanism on molecular level in electrohydrogenation reaction of FF. The effect of electrode material, applied potential, and electrolyte composition on adsorption orientation of different moieties on the catalyst surface was investigated. The tendency of educt and product to approach the electrode surface, as well as the availability and dynamics of hydrogen bonding was examined by MD simulations. Raman spectroscopic measurements deliver first insights into the surface processes while also contributing a basis for the verification of the MD simulations. These simulations then provide more detailed information that is not accessible with experimental methods. In this way, the utilized methods complement each other.

In both, the methods and results sections, first the spectroelectrochemical experiments will be presented, before the MD simulation are discussed. Both are then resumed in a mutual conclusion.

Methods

Experiments

Chemicals

Electrolyte solutions for spectroelectrochemcial experiments were prepared with bidestilled water (Carl Roth, Germany), KCl (99%, Carl Roth, Germany), suprapur sulfuric acid (96%, Sigma–Aldrich, Germany), hydrochloric acid (37%, Carl Roth, Germany), FF (99%, Sigma–Aldrich, Germany), MF (99%, Sigma–Aldrich, Germany), and FA (98%, Sigma–Aldrich, Germany). Before utilization nitrogen was bubbled through the electrolyte solutions for 15 min to remove oxygen. For electrochemical performance experiments the same organic compounds were used, while the electrolyte components were deionized water, sulfuric acid (95%, Sigma–Aldrich, Germany), and acetonitrile (99.9% HPLC grade, Sigma–Aldrich, Germany). The acetonitrile was utilized to reduce evaporation of volatile compounds.

Spectroectrochemical Experiments

Spectroelectrochemical experiments were carried out under the utilization of Raman spectroscopy with an InVia Reflex Raman confocal microscope (Renishaw plc, UK) combined with a 785 nm (diode, 300 mW) and 532 nm (Nd:Yag, 50 mW) laser. The Raman shift was calibrated with a silicon reference at 520.5 cm^{-1}. WiRe 5.0 software (Renishaw plc, UK) was used to obtain the spectra, remove cosmic rays and perform a polynomial background correction. A modified Raman Electrochemical Flow Cell (Redox.Me, Sweden) with a volume of 4.5 mL and an electrode area of 3.5 cm^2 was used in combination with a water immersion objective (HCX APO L 20×, 0.5 NA W U-V-I-/D 3.5, Leica Microsystems, Germany). Electrochemical procedures and measurements were performed with an SP-150 Potentiostat (BioLogic SAS, France) in combination with a RE-1B 3 M NaCl Ag|AgCl (BioLogic, France) reference electrode, Pt wire (99.9%, Redox.Me, Sweden) as counter electrode and Cu (99.995%, ChemPur, Germany) and Ag (99.995%, ChemPur, Germany) as working electrode. As the first preparation step the electrodes were ground with abrasive paper and polishing diamond (1 μm) and alumina (0.05 μm). The SERS (surface-enhanced Raman spectroscpy) effect for the copper working electrode was generated by performing 20 ORCs (oxidation-reduction-cycles) between −0.2 V and 0.9 V vs. Ag|AgCl with 20 mV/s in 0.1 M KCl aqueous solution without electrolyte flow. Ag working electrodes were prepared similarly with ORC according to a literature procedure in 0.1 M KCl.[29] After the roughened surface was generated, the electrolyte feed was changed to the respective acidic electrolyte, and subsequently, a constant potential of −0.1 V vs. Ag|AgCl was applied to reduce metal oxide species from the surface generated during the ORC. Afterward, a background spectrum was acquired before the respective starting material was added to the electrolyte feed. For this purpose, an Ismatec Reglo Digital peristaltic pump (Cole-Parmer, USA) in combination with PTFE and Viton tubes was used with a flow rate of 1 mL/min. Afterwards, a spectrum under OCP (open circuit potential) conditions was acquired. The working electrode potential was subsequently varied, and spectra were acquired at each potential step. For the spectrum acquisition, an extended mode between 400 and 3500 cm^{-1} was used with 10 s exposure time and 1 accumulation. Regions irrelevant for the evaluation are not depicted for clearer visibility. Only vibrations caused by the electrolyte could be observed in the omitted regions. Furfural C–H stretching vibrations (typically higher wave numbers than 3000 cm^{-1}) were not visible due to their low signal intensity. For comparison, SI Figure S1 shows an exemplary complete spectrum. The confocal mode of the Raman microscope was employed. For measurements on Ag working electrodes, the 532 nm laser was employed, while the 785 nm laser was used for Cu working electrodes. The different laser wavelengths are necessary for the SERS effect of the respective electrode materials. However, as this difference can influence the relative intensity of the Raman signals, only qualitative analysis was performed. Solution spectra were obtained from 0.5 M starting material solutions in 0.1 M H_2SO_4 solution. Due to the low solubility of MF, neat MF was used as reference instead of solution spectra. In these cases, the confocal mode was not employed. For surface spectra, the utilized acquisition parameters, and used FF concentration, no FF signal from solution can be measured, indicating FF signals originating from the surface. Signals were assigned according to the literature.[30,31]

Electrochemical Experiments

Reaction performance experiments were carried out for 2 h at room temperature in divided H-type cells at an electrode potential of −0.76 V vs. RHE (reversible hydrogen electrode) (measured vs. Ag/AgCl sat. KCl, SE11, Sensortechnik Meinsberg, Germany) with 12 cm^2 contact area of the ground and rinsed Ag (99.9%, ChemPUR, Germany) and Cu (99.95%, ChemPUR, Germany) electrodes with the electrolyte solution (0.5 M aqueous H_2SO_4 solution with 85% deionized water and 15% acetonitrile). Pt (99.9% ChemPUR, Germany) was used as counter electrode. Each half cell contained 50 mL solution, while they were separated by a cation exchange membrane (fumasep FKE-50, Fumatech, Germany). The more negative potential for the bulk electrolysis experiments in comparison to spectroelectrochemical was necessary for a sufficient conversion for a measurable concentration difference. The starting material concentration was 0.05 M. Product concentrations were analyzed with HPLC using an Agilent 1260 Infinity II LC (USA) with a Phenomenex synergi Hydro-RP 80 Å column (4 μm, 250×4.6 mm) and a diode array detector. A 1:1 mixture of deionized water and acetonitrile served as eluent at 25 °C with a 1 mL/min flow rate.

MD Simulations

All MD simulations in this work were performed with LAMMPS using version 7. Aug 2019[32] and GROMACS[33] version 2019.06. The educt and the product (FF and MF) as well as sulfate ions in the system were modeled using OPLS-AA force field.[34] The utilized force field models for educts and products were described in detail in our previous work.[35] The OPLS-AA Lennard-Jones parameters from Halstead et al.[36] were exploited for modeling chloride ions. TIP3P[37] force field was employed to model water molecules where hydronium ions were modeled using parameters from Wolf et al.[38]

The metallic electrodes consisted of Cu or Ag atoms where the (100) face was in contact with the electrolyte. The Lennard-Jones parameters and cell parameters of metallic electrodes were taken from the interface force field by Heinz et al.[39]

GROMACS Simulations

GROMACS was used for simulations of the potential of mean force (PMF). Here, PMF describes the binding affinity of a solute to the electrode surface. A reaction coordinate connected the reference state at the surface of the electrode with the end state in z direction. The end state was in sufficient distance within the bulk phase to minimize the effect of the electrode. The number of atomic Cu and Ag layers used to model the electrode slabs was chosen in a way that the resulting layer thickness was larger than

the cut-off radius. The bulk phase consisted of one solute molecule (i.e. FF, MF) in water as solvent. The simulations started with an equilibration for the bulk phase in the NPT ensemble at 298.15 K and 1 atm to calculate the density and proper box size for the following PULL and PMF simulations. Subsequently, PACKMOL[40] was used to create the liquid bulk phase. The initial configuration for the PULL simulation was completed by inserting the electrode. A 0.5 fs time step was considered for all simulations. Both PULL and PMF simulations were conducted in the NVT ensemble with a time constant for coupling temperature of 2.5 ps. The coupling value was selected based on the recommendations in the GROMACS manual and the reported literature value.[41] All simulations were performed using leap-frog dynamic integrator with the embedded thermostat. The electrostatic interactions were solved using Particle Mesh Ewald electrostatics (PME),[42] and a 12 Å cut-off was considered for Lennard-Jones and electrostatic interactions. The SETTLE[43] algorithm was used to impose constraints to model water as a rigid molecule. In order to sample configurations along the transition path, the movement of the solute along the reaction coordinate was biased by a harmonic umbrella potential with the pull rate of 0.005 nm/ps, and a force constant of 5000 kJ/(mol × nm^2). The PULL simulation was conducted to generate the initial configurations for the equilibration simulation of every umbrella state. The equilibration simulation for each state was performed for 0.5 ns while the solute molecule was fixed using a significantly high force constant for the biasing potential. The umbrella sampling method[44,45] was used for PMF determination. To ensure sufficient histogram overlap, a varying number of 18 to 30 different umbrella states were introduced for the different simulated systems. All systems were sampled up to a distance of 3 nm from the electrode surface in the liquid bulk phase. Each state was executed in the production phase for 3 ns with the force constant of 600 kJ/(mol × nm^2) for the biasing potential. Consequently, the Weighted Histogram Analysis Method (WHAM)[46,47] was employed for the evaluation of the full PMF, while the bootstrapping method was utilized for uncertainty estimation.

LAMMPS Simulations

The simulated electrochemical cell was composed of two parallel metallic electrodes and a liquid electrolyte in between. A schematic view of a simulated cell is shown in Figure 2a, together with the nomenclature of relevant atom types in FF in Figure 2b.

Three electrolyte compositions were considered in the simulation: (1) aqueous solution of FF with 0.5 M concentration (indicated by Aq suffix), (2) 2 M of completely dissociated sulfuric acid in hydronium ions and sulfate ions, and 0.5 M of FF in water solution (H_2SO_4 suffix), (3) 4 M of completely dissociated hydrochloric acid in hydronium ions and sulfate with the 0.5 molar concentration of FF (HCl suffix). In the experiment at high concentration H_2SO_4 solution, there was a constant equilibrium between hydrogen sulfate and sulfate ions. However, to reduce the complexity of the simulated systems in the MD study, a complete dissociation of H_2SO_4 was assumed. Moreover, the higher concentration of FF and acid was considered to provide sufficient samples for statistically accurate analyses of MD simulations. A 0.5 fs timestep was used for all simulations, while the temperature and pressure were controlled with Nose-Hoover thermostat and barostat[48,49] with 50 fs and 500 fs damping parameters for temperature and pressure. The damping values in the LAMMPS simulations were selected based on the recommendations in the software manual. In each simulation, before placing the liquid phase between the electrodes, the liquid phase was equilibrated at 298.15 K and 1 atm with fixed sizes of the simulation box in x and y directions. The hydronium ions were constrained by SHAKE[50] algorithm. The equilibration was performed for 2 ns in NPT ensemble after a minimization with conjugate gradient algorithm. Consequently, the equilibrated length of simulation box in z-direction from this step was utilized as the distance between two electrodes in further simulations in a full electrochemical cell system. The electrodes consisted of five atomic layers, with the first layer located at z = 0 Å. Due to the various sizes of the cell parameters for different metals, the resulting sizes of the simulated cells slightly differ from each other (SI, Table S3). The polarizable electrode model by Petersen et al.[26] was used to model an electrochemical cells at constant potential. Periodic boundary conditions were set for the simulation box in two directions (x and y), while a fixed boundary condition was used in the perpendicular direction to the electrodes (z-direction). The particle-particle particle-mesh solver (PPPM)[51] with 1×10^{-5} accuracy was employed for the calculation of long-range electrostatic interactions. The slab command in LAMMPS was used to virtually insert an empty volume (12 Å in z-direction) between the electrode to turn off the interactions between them. The Lennard-Jones interactions and electrostatic interactions were calculated with 12 Å cut-offs. After placing the liquid phase between two electrodes, a conjugate-gradient minimization was conducted, which was followed by a system annealing at 1000 K with an NVT ensemble for 3 ns. The system subsequently was quenched for 1 ns to 298.15 K and the NVT simulation was carried out for 8 ns. From the 8 ns simulations, the first 3 ns were considered as equilibration and the last 5 ns of the simulation was accounted as a production phase. All simulations were performed in four different potentials between the electrodes (i.e. 0 V, 1.5 V, 3.5 V, and 8 V) to examine the effect of applied voltages. The corresponding voltages on the working electrode were equal to the half of the applied cell voltages (i.e. 0 V, −0.75 V, −1.75 V, and −4 V). It should be noted that the applied voltages in MD simulations are not directly relatable to the potential differences in the experiments due to the various losses in reality. Accordingly, only the trends of applied potential differences in MD simulations and experiments can be compared.

Each simulation for an individual system was repeated three times from completely independent initial configurations and velocity random seeds for a better statistic. The trajectory in the production phase was generated every 100 time steps (i.e. 50 fs) for visualization using OVITO[52] or further various post-processing. Post processing of trajectories was done using VMD[53] for RDF calculations, TRAVIS[54,55] for analyzing the hydrogen bonding, and in-house tools for determination of the educts' orientation at the electrode surface.

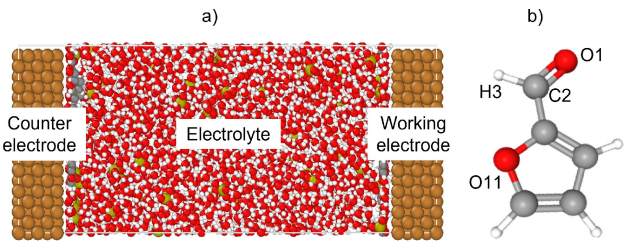

Figure 2. a) Setup configuration of a simulated electrochemical cell with LAMMPS, b) molecular structure of FF with naming of atoms.

Results and Discussion

Spectroelectrochemical Experiments

For an experimental evaluation of the interaction of FF with metal surfaces *in situ* electrochemical Raman spectroscopy was employed. Measured spectra of FF in aqueous solution were comparable to literature and assigned accordingly.[30] First the standard case of adsorption of FF in sulfuric acid solution on Cu under OCP conditions will be discussed before the effect of a change in electrolyte concentration, Ag electrode instead of Cu electrode, potential changes, and variation in the electrolyte anion are considered.

Adsorption on Copper

A comparison of solution spectra and spectra on Cu metal surfaces shows comparable signals (Figure 3a and b), yet differences can be observed. First, most Raman signals shift to a lower wavenumber and vibration energy for the surface bond species (SI, Table S1), indicating an interaction between molecule and metal surface. The changes for the ring vibrations are in the range of 2–15 cm^{-1}. Although sometimes these shifts are classified as a result of chemisorption, while physisorbed species remain unshifted,[56] our interpretation follows other groups suggesting lower band shifts resulting from physisorbed species, while chemisorbed species shift with a larger difference.[57] The physisorption of the furan ring on the surface is also in accordance with an ATR-SEIRAS study by Anibal et al.[18] The interaction between the furan ring and Cu surface is the first indication for parallel or tilted ring orientation. Additionally and most apparent when comparing solution and surface spectra, the aldehyde stretching vibration at 1666 cm^{-1} seems to be strongly attenuated (Figure 3a and b, red highlighted region) as already described for FF on Cu and Ag surfaces in pH 3 and 7 environments.[19,56] This observation can be ascribed to a stronger FF/metal interaction, accompanied by a hydrate formation of the carbonyl group.[58] Furthermore, an additional signal at 1605 cm^{-1} respectively 1608 cm^{-1} (Figure 3a and b, green highlighted region) coinciding with a 1585 cm^{-1} signal present in measurements without FF (SI, Figure S2), likely originating from a water bending vibration, can be observed.[59] This signal could be the strongly shifted aldehyde stretching vibration, indicating chemisorption of the aldehyde group or the carbonyl hydrate band resulting from strong carbonyl-metal interaction as suggested by Jia et al.[56] The presented data at

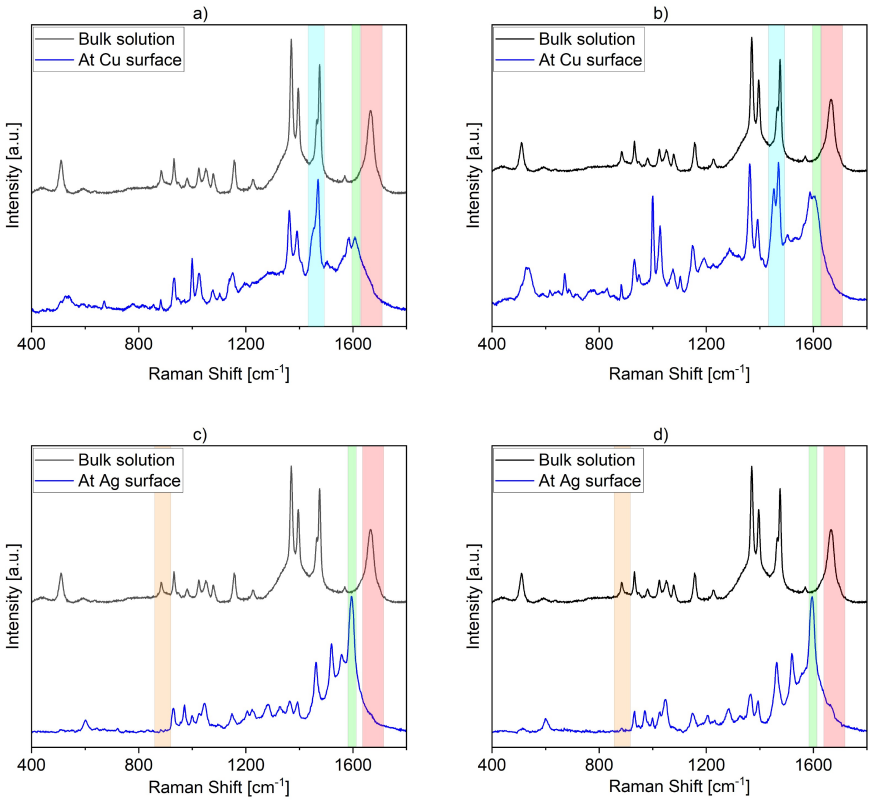

Figure 3. Comparison of bulk solution (all black) and surface (all blue) Raman spectra. Bulk solution spectrum was acquired from 0.5 M FF solution. Surface spectra were acquired from 0.05 M FF solution in a) 0.1 M H_2SO_4 solution on a Cu surface, b) 0.5 M H_2SO_4 on a Cu surface, c) 0.1 M H_2SO_4 on a Ag surface, and d) 0.5 M H_2SO_4 on a Ag surface. Red highlighted region: aldehyde stretching vibration (1666 cm^{-1} in bulk solution), green highlighted region: carbonyl hydrate vibration (1605 cm^{-1} at surface), blue highlighted region: C=C stretching vibration (1475 cm^{-1} (*trans*-FF), 1466 cm^{-1} (*cis*-FF) in bulk solution), orange highlighted region: out of plane ring vibration (884.1 cm^{-1}).

pH 0–1 are comparable to the results at pH 3 published by the group of N. Kornienko.[19]

Adsorption on Silver

The respective spectra of FF on Ag surfaces (Figure 3c and d) on the other hand show a different behavior. The presence of band shifts (SI, Table S2) in the range of 1–13 cm^{-1} in relation to the FF solution spectra indicate a physisorption of FF on the Ag surface comparable to the adsorption on Cu (see section Adsorption on Copper). The attenuation of the aldehyde C=O stretching vibration is comparable to literature[56] and measurements on Cu (see section Adsorption on Copper), indicating a strong interaction between aldehyde group and metal surface. Comparably to FF on Cu a new signal at 1594.8 cm^{-1} respectively 1596 cm^{-1} emerges (Figure 3c and d, green highlighted region), presumably arising from a strong shift due to chemisorption of the aldehyde bond or due to the proposed hydrate formation.[56] Apart from the similarities, both spectra from Cu and Ag show considerable differences in the relative signal intensities. The spectra also deviate from FF adsorption spectra in Ag colloid solution, suggesting an orientation perpendicular/tilted towards the surface.[56] As depicted in Figure 3c and d (orange highlighted region), the out-of-plane vibration at 884.1 cm^{-1} in the solution spectrum is almost extinguished in the surface spectra. Here we assume in accordance to the Raman surface selection rules[60] a tilted orientation of FF, which is more perpendicular towards the surface than for Cu, but still allows interaction of furan ring and metal surface. Deviations from the literature spectra[56] are assumed to originate from differences in surface geometry and therefore different adsorbate alignments.

Electrolyte Concentration

A remarkable observation can be made by comparing the FF C=C stretching vibration in bulk solution at 1475 cm^{-1} with their surface equivalents in 0.1 M and 0.5 M sulfuric acid solution on Cu (Figure 3a and b). FF has two conformers: *cis* and *trans*.[61] While the *cis*-conformation has both oxygen atoms pointing in the same direction, the *trans*-conformation has the aldehyde-oxygen close to the ring. For this reason, the main signal at 1475 cm^{-1} (*cis*) is accompanied by a smaller signal at 1466 cm^{-1} (*trans*) (Figure 3a and b, blue highlighted region).[62] Other signals originating from the differences of *cis*/*trans* conformers are either not visible due to the low intensity of the respective signal or do not develop a distinguishable signal. On the surface for 0.5 M sulfuric acid solution, the intensity of the *trans*-signal is increased relative to the *cis*-signal, suggesting a higher portion of molecules in *trans*-conformation, while the *cis*-conformation is still the preferred one. Although there is typically an equilibrium at room temperature between the energetically higher *cis*-conformation and the energetically lower *trans*-conformation, the equilibrium is on its *cis*-side dissolved in electrolyte under ambient conditions and adsorbed on metal surfaces.[62,63] The higher electrolyte concentration seems to influence the molecules close to the surface in a way that leads to a preference of the energetically lower *trans*-conformation, possibly due to changed interactions in hydrogen bonding. A comparison of the measurements with different electrolyte concentrations on Ag reveal comparable spectra that do not indicate concentration dependencies.

Potential Changes

After the preceding experiments showed the adsorption behavior on the metal surface at OCP, potential variations were investigated. Subsequent potential changes on Cu from 0.2 V vs. RHE towards negative electrode potentials of −0.8 V vs. RHE lead to a change in the resulting spectra (Figure 4a and b, potentials more negative than −0.5 V vs. RHE omitted due to unchanged spectra and low overall intensity). The sulfuric acid concentration does not seem to have a substantial influence on the potential-dependent surface adsorption process of FF, as both spectra sets look comparable. With more negative potentials the relative intensity of the hydrate signal at 1608 cm^{-1} increases, while it is also blueshifted to 1613 cm^{-1} (Figure 4a and b, green highlighted region). This behaviour was already described for water molecules during hydrogen evolution reaction.[59] Furthermore, the overall intensity of the spectra changes. From 0.2 V to −0.2 V an increase can be observed until it decreases substantially. The initial increase can be explained by reaching the potential of zero charge, where a maximum surface concentration of neutral compounds would be expected.[12] Furthermore, reorientation (as consequence from approaching the potential of zero charge) can explain this behavior.[12] The subsequent signal decrease can be attributed to an increasing distance between FF and the surface and a decay of the roughened surface and therefore a loss in enhancement.[64] Additionally, comparable to the observed rotational differences between FF on Cu surfaces with 0.1 M and 0.5 M sulfuric acid (see section Electrolyte Concentration) with more negative potential, the *trans*-configuration seems to be more favored within the equilibrium. Product formation can only be observed at the signal emerging at 1503 cm^{-1} (Figure 4a and b, red highlighted region), as apart from this band all other product bands coincide with FF signals (SI, Figure S5).[19] The peak can be attributed to both FA and MF. It is already slowly emerging at a potential of 0 V to −0.1 V and increases relative to the overall spectrum steadily, until it becomes one of the dominating signals at −0.5 V. This increase in signal intensity corresponds to an increase in production rate with more negative potentials. At a shift of 2264 cm^{-1} (Figure 4a and b, blue highlighted region) a Cu–H vibration can be observed comparable to the Pt–H formation described in the literature,[65] indicating a reduction of protons. At more negative potentials this signal increases relative to the overall spectrum as more surface hydrogen is formed. The Cu–H formation can also be observed in the absence of FF (SI, Figure S3) where the signal is easier to differentiate from the background, since the overall intensity is smaller and the surface is not blocked from

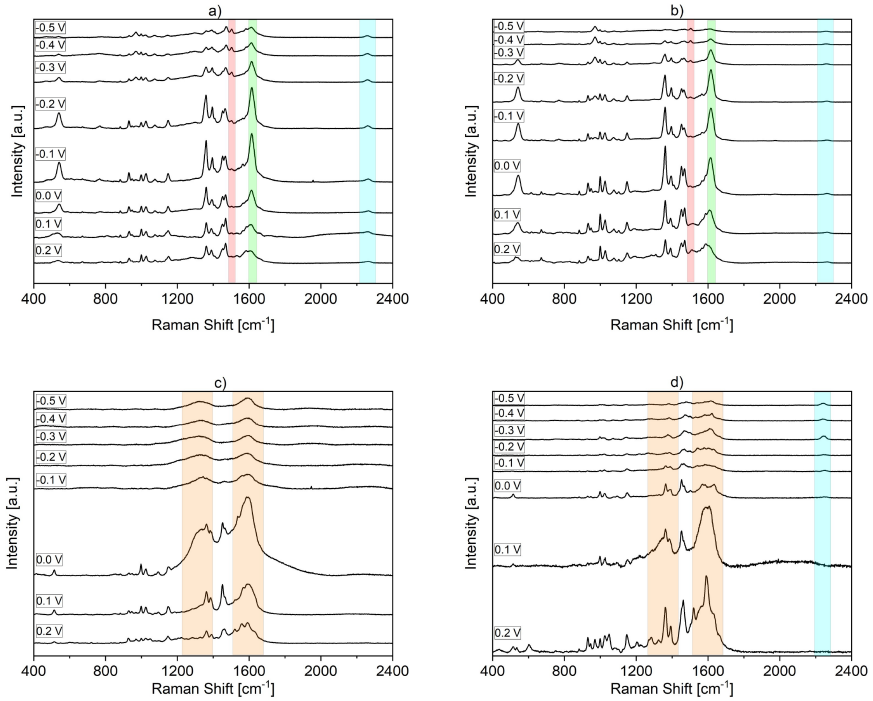

Figure 4. Surface spectra of FF with varying potentials a) in 0.1 M H_2SO_4 solution on a Cu surface, b) in 0.5 M H_2SO_4 solution on a Cu surface, c) in 0.1 M H_2SO_4 solution on an Ag surface, d) in 0.5 M H_2SO_4 solution on an Ag surface, with potentials given vs. RHE. Red highlighted region: product formation (MF and FA) (1503 cm^{-1}), green highlighted region: carbonyl hydrate vibration (1605 cm^{-1}), blue highlighted region: Cu–H/Ag–H stretching vibration (2264 cm^{-1} (Cu–H), 2246 cm^{-1} (Ag–H)), orange highlighted region: vibration of the electrolyte (1591 cm^{-1} and 1340 cm^{-1}).

adsorbed FF. These findings support hydrogen as electron carrier for reduction as a plausible mechanism.[8]

Comparing the results for potential changes on Cu with those on Ag (Figure 4c and d) reveals in the beginning of the potential steps a similar increase of the hydrate signal as already observed for Cu. Already at mild negative potentials the bands of FF are increasingly obscured by two dominant signals at 1340 cm^{-1} and 1591 cm^{-1} (Figure 4c and d, orange highlighted region) that can also be observed in the respective measurements without FF (SI, Figure S2). This indicates a higher interaction of the electrolyte/water system with the Ag surface than FF exhibits causing a higher distance between molecule and electrode surface. This behavior can be explained by a lower binding energy between FF and Ag than for Cu which was previously described.[66] For a higher electrolyte concentration of 0.5 M (Figure 4d) the FF bands can be observed longer before they are blocked by the electrolyte signals and occasionally reappear after e.g. a small movement with the microscopic stage causing small disturbances in the electrochemical double layer, leading to a renewed approximation of FF to the Ag surface. This behavior can not be observed for 0.1 M sulfuric acid electrolyte. Comparing the reaction performance parameters (Table 1) for Ag and Cu a difference in reaction performance can be observed. While Ag shows a better conversion it exhibits a poorer mole balance followed by poorer product selectivities and Coulomb efficiencies. This could be attributed to a higher rate of side reactions like e.g. the oligomerization that furanic compounds typically undergo.[6] In

Table 1. Reaction performance parameters for the electrochemical hydrogenation of FF at −0.76 V vs. RHE on Cu and Ag electrodes obtained from H-cell experiments in 0.5 M H_2SO_4 solutions containing 15% acetonitrile.

	Cu electrode	Ag electrode
Conversion [%]	60.2	99.2
Mole balance [%]	87.7	45.5
Selectivity FA [%]	19.9	8.9
Selectivity MF [%]	59.9	36.1
Coulomb efficiency FA [%]	11.0	3.0
Coulomb efficiency MF [%]	65.8	24.1
Overall Coulomb efficiency [%]	76.8	27.0

context of the Raman experiments the reaction performance can be a result of the lower binding energy, leading to a shorter contact time with the electrode surface. This consequently leads to incomplete reaction products that due to their instability easier undergo side reactions. Comparing these results to the analogical molecule HMF on Ag that showed better efficiencies and selectivities shows that despite their similarities there seems to be a difference in their reactivity.[67] FF as starting material on Ag, on the other hand, was not closer investigated, yet.[66] Comparable to the spectra on Cu, product formation can be observed through the signal at 1510 cm^{-1}, with the signals starting to emerge at a potential of 0 V. A Ag–H formation can also be observed at a Raman shift of 2246 cm^{-1} (Figure 4d, blue highlighted region). In contrast to Cu, the signal is first visible at a potential of 0 V, while the Cu–H signal could even be observed with no potential applied. With more negative

potential the Ag–H signal is increased relative to the overall spectrum, comparable to the respective Cu–H experiment.

Anion Influence

In order to investigate the anionic influence on the molecule-metal interaction, the same experiments were conducted with HCl solution as electrolyte. The resulting spectra (Figure 5) show in comparison to those presented in Figure 3 relatively low signal intensity and poor signal-to-noise-ratio for both metals Ag and Cu. This behavior possibly originates from a higher distance between molecule and electrode caused by a decreased electrode affinity and increased electrolyte affinity in the respective electrolyte. Typically chloride salts are used for SERS substrate to stabilize nanoparticle structures and avoid surface restructuring by chloride adsorption on the surface, which in this case potentially block the FF more than with sulfate as anion.[68] This result correlates with a slightly poorer reaction performance for HCl as electrolyte in comparison to H_2SO_4 explainable by a larger distance between molecule and surface, although the reaction performance does not drop as much as possibly anticipated by the Raman spectra, again emphasizing an outer-sphere mechanisms.[6] This difference between Raman experiments and reaction performances needs to be investigated more thoroughly, also considering the influences on the SERS effect of different parameters.

The signals that could be observed are comparable to the spectra in sulfuric acid electrolytes. Due to the high number of hardly recognizable signals and poor signal-to-noise-ratio a further analysis was not performed. The analysis of potential changes (SI, Figure S4) reveals similar unsteady spectra for Ag (see section Potential Chanes), while the changes in the spectra for Cu remain consistent. Again, this observation can be accounted to a higher binding energy for FF on Cu than for Ag.

MD Simulations

PMF Simulations

The PMF curves were calculated for educts and products at different electrode materials. The PMF curves for FF and for MF systems at Cu and Ag electrodes are presented in Figure 6. As shown in this figure, the FF has higher binding energy values than MF for both electrode materials. This behaviour indicates the stronger tendency of educts to approach the electrode surface compared to products when both are available in the interface layer. The tendency of educts towards electrode surface is necessary for initiating and proceeding reaction on the electrode surface. Moreover, the FF molecules have higher

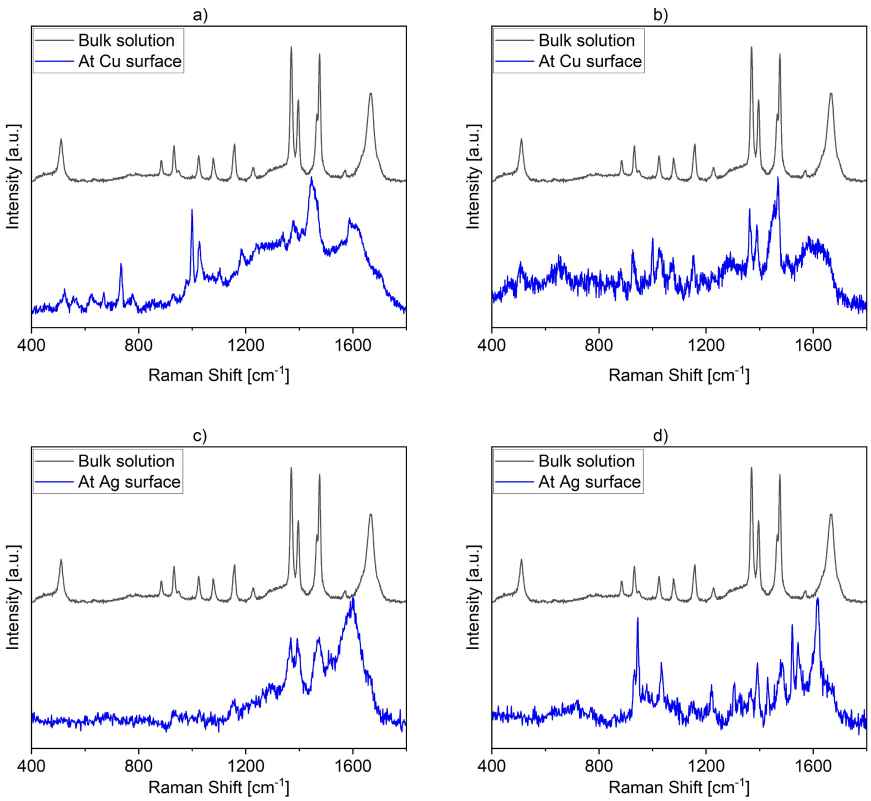

Figure 5. Comparison of bulk solution (all black) and surface (all blue) Raman spectra. Bulk solution spectrum was acquired from 0.5 M FF solution. Surface spectra were acquired from 0.05 M FF solution in a) 0.1 M HCl solution on a Cu surface, b) 0.5 M HCl on a Cu surface, c) 0.1 M HCl on a Ag surface, and d) 0.5 M HCl on a Ag surface.

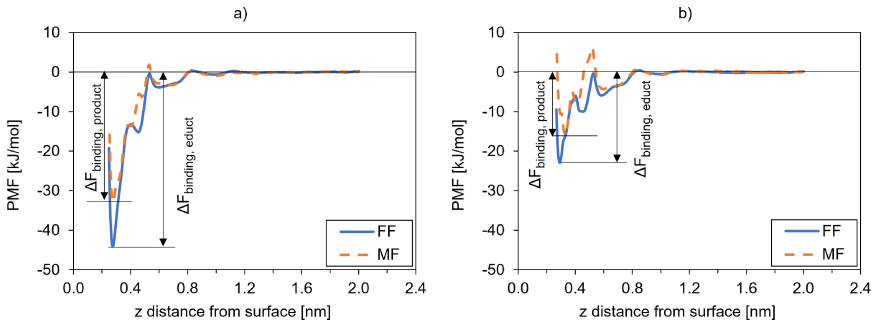

Figure 6. PMF curves of FF and MF at a) Cu electrode and b) Ag electrode versus the distance of solute from the electrode surface. $\Delta F_{binding,educt}$ and $\Delta F_{binding,product}$ show the binding free energy of educt and product, respectively.

binding affinity to the Cu electrode in comparison to the Ag electrode. These results are consistant with the findings from DFT calculation in Ref. [63,66] and in agreement with the observations from experiment (see section Potential Changes). The positions of the minima in the PMF curves in Figure 6 indicate the equilibrium distance of the solute molecule from the electrode surface in the simulated systems. The equilibrium distance of FF molecule from the surface was extracted from Figure 6a for Cu electrode as 0.275 nm and Figure 6b for Ag electrode as 0.294 nm. Thus, the distance between FF molecules and the electrode surface is smaller for Cu in comparison to Ag electrode, which also accords with the observation from experiment (see section Potential Changes).

In order to provide an insight into the binding affinity of the educts in comparison to the products, the binding free energies ($\Delta F_{binding}$) of educts and products were extracted from the PMF curve. Subsequently, the binding affinity difference of each educt/product pair was calculated by:

$$\Delta\Delta F_{binding} = \Delta F_{binding,educt} - \Delta F_{binding,product} \quad (1)$$

The resulted values for $\Delta\Delta F_{binding}$ of the educt/product pair are equal to -11.24 ± 2.29 kJ/mol and -6.98 ± 2.67 kJ/mol for Cu and Ag electrodes, respectively. The $\Delta\Delta F_{binding}$ is more significant for the copper electrode, which shows more substantial binding energy of the educt in comparison to the product for this electrode. Though, it should be noted that these calculated binding free energies only present an estimation of the actual binding energies due to the required simplifications in both the simulation method and molecular models.[69] However, we aimed to provide a qualitative comparison between the binding affinity of educts and products at both electrodes. Due to the likeliness of the studied systems, the errors for $\Delta F_{binding}$ in all systems are expected to be similar.

Furfural Configuration at the Working Electrode

The geometry configuration of educts at the working electrode (WE) is an important characteristic, which can also define the reaction path on the surface. Therefore, the orientation of FF molecules in the vicinity of electrode surface was quantified by the so called S factor:

$$S = \left\langle \frac{1}{N} \sum_{i=1}^{N} \frac{1}{2} (3 \cos^2 \theta_i - 1) \right\rangle \quad (2)$$

where N is the number of FF molecules and θ is the angle between the normal vector of furan ring and the normal vector of electrode surface. According to this definition, S has a value between -0.5 and 1.0, where the 1.0 value indicates a parallel orientation of the furan ring to the surface and -0.5 refers to a perpendicular orientation. Figure 7 exemplary shows the various possible furan ring configurations towards an electrode surface.

For this analysis, the space between two electrodes was divided into fourteen layers, and for each layer the S factor was calculated and averaged during the production phase. The S factors of FF for the last layer adjacent to the working electrode (cathode) with and without ionized acids are presented in Figure 8.

Figure 8 illustrates that for all simulated copper systems (i.e., Aq, HCl, H_2SO_4) in both zero and 1.5 V cell voltages, the preferable orientation of the FF is nearly parallel ($S = 1$) or tilted with a slight angle ($\theta < 20^\circ$) to the surface. Studies in the literature[20–22] have also shown that this parallel orientation can lead the reaction to a decarbonylation of FF to furan or hydrogenation of FF to FA and MF. Results from this work

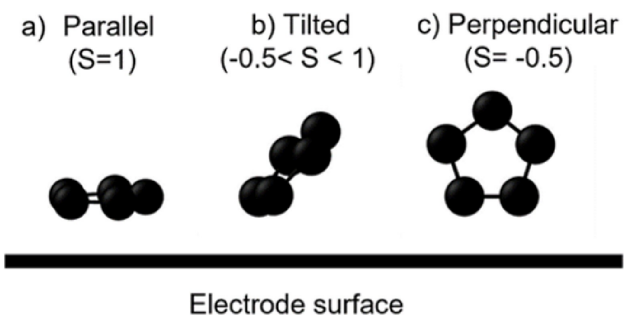

Figure 7. Orientations of a furan ring towards an electrode surface.

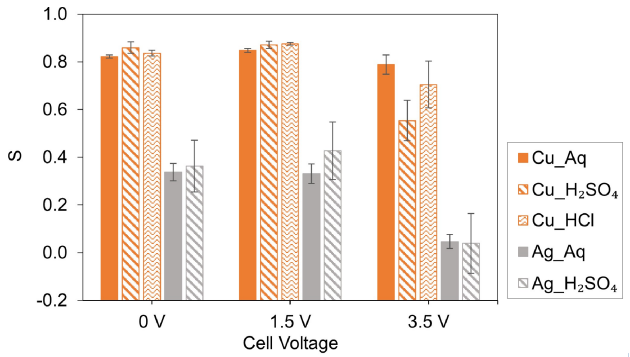

Figure 8. S factor for FF at the copper and silver working electrode at different potential differences between electrodes (0 V, 1.5 V, 3.5 V) for aquous (Aq) system, ionized sulfuric acid and ionized hydrochloric acid system.

reflect the DFT calculation findings from literature,[22] which showed that the most stable configuration for adsorption of FF on the copper is the parallel one. This result also corroborates the findings from the Raman spectroscopy for sulfuric acid (see section Adsorption on Copper).

As can be seen in Figure 8, there were no significant changes in orientation of FF molecules detected by changing anions to chloride in Cu systems. However, the Raman spectroscopy detected a poor signal-to-noise-ratio (see section Anion Influence), which prevented detailed orientation analysis.

For the silver electrode, the FF molecules approach with a higher angle to the electrode surface ($\theta > 35°$), which may affect the electrode's reaction path. This more tilted orientation of FF at the silver electrode also agrees with our earlier observations in experiments (see section Adsorption on Silver). This attitude seems to be related to the lower binding energy of FF adsorption on the silver electrode in comparison to the copper electrode, which was reported from PMF calculation (see section PMF Simulations). The S factor has the highest value at 1.5 V potential in all simulated systems for Cu and Ag electrodes. However, increasing the potential difference between the two electrodes to 3.5 V results in a reduction of the S factor, indicating a more tilted adsorption configuration for FF molecules. This behaviour is consistent with the reported trend also from Raman spectroscopy (see section Potential Changes).

Figure 9 presents a snapshot of the simulated systems at the high applied potential between two electrodes (i.e. 8 V). As shown in Figure 9 for all simulated systems, most FF molecules adsorbed outside the inner Helmholtz layer. In other words, the adsorbed ions of the electrolyte on the surface prevent the FF molecules to react with the metallic electrode. This finding also agrees with the outcome from the experiment at potentials more negative than −0.5 V vs. RHE, which suggests that applying a significantly large potential difference has an adverse effect on proceeding of the reaction. Therefore, we exclude the high voltage simulations from other investigations at the electrode surface.

The structural analysis of simulated systems were complemented by calculating number densities of different atoms in the FF molecules according to the distance from WE to provide a deep insight into their adsorption configuration on the electrode surface. The density profiles for O1, C2, H3 atoms in aldehyde group and O11, the oxygen atom in the furan ring, were calculated and averaged over the production phase of each simulation (Figure 2b for atomic indices). The computed density profiles were normalized to the average number of adsorbed molecules on the surface for each simulation. Subsequently, the average values and the uncertainties for the normalized density profiles were computed for all repetition of each system according to the distance from WE. The density profiles are presented in Figure 10 and Figure 11 for O1, C2, H3 atoms in aldehyde group and O11, the oxygen atom in the furan ring.

The density profile curves for the Cu systems are presented in Figure 10. They illustrate that at zero voltages for the aqueous (Figure 10a) and the H_2SO_4 (Figure 10d) systems, the highest peaks can be observed for the O1, C2 atoms at the same distance from the surface and quite the same intensity. In the HCl system at zero voltage (Figure 10g), a separation can be seen between the peaks of the C2 curve and O1 in a way that the O1 peak occurs closer to the WE. A possible explanation for this might be the bigger size of sulfate anions in comparison to chloride ions. In these systems, both anions and cations are available on the WE in order to balance the charges in the

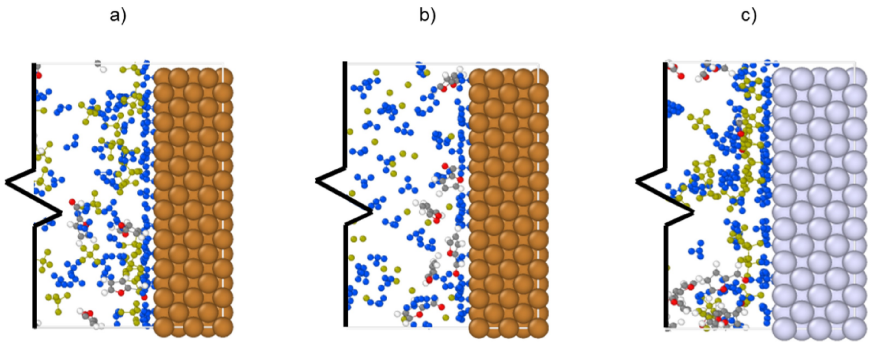

Figure 9. The snapshots of the simulated systems at the vicinity of working electrode with a) Cu electrodes in H_2SO_4 solution, b) Cu electrodes in HCl solution, and c) Ag electrodes in H_2SO_4 at 8 V applied potential difference between two electrodes. Water molecules were deleted for better visualisation, the yellow ions represent anions of the electrolyte, blue ions represent cations.

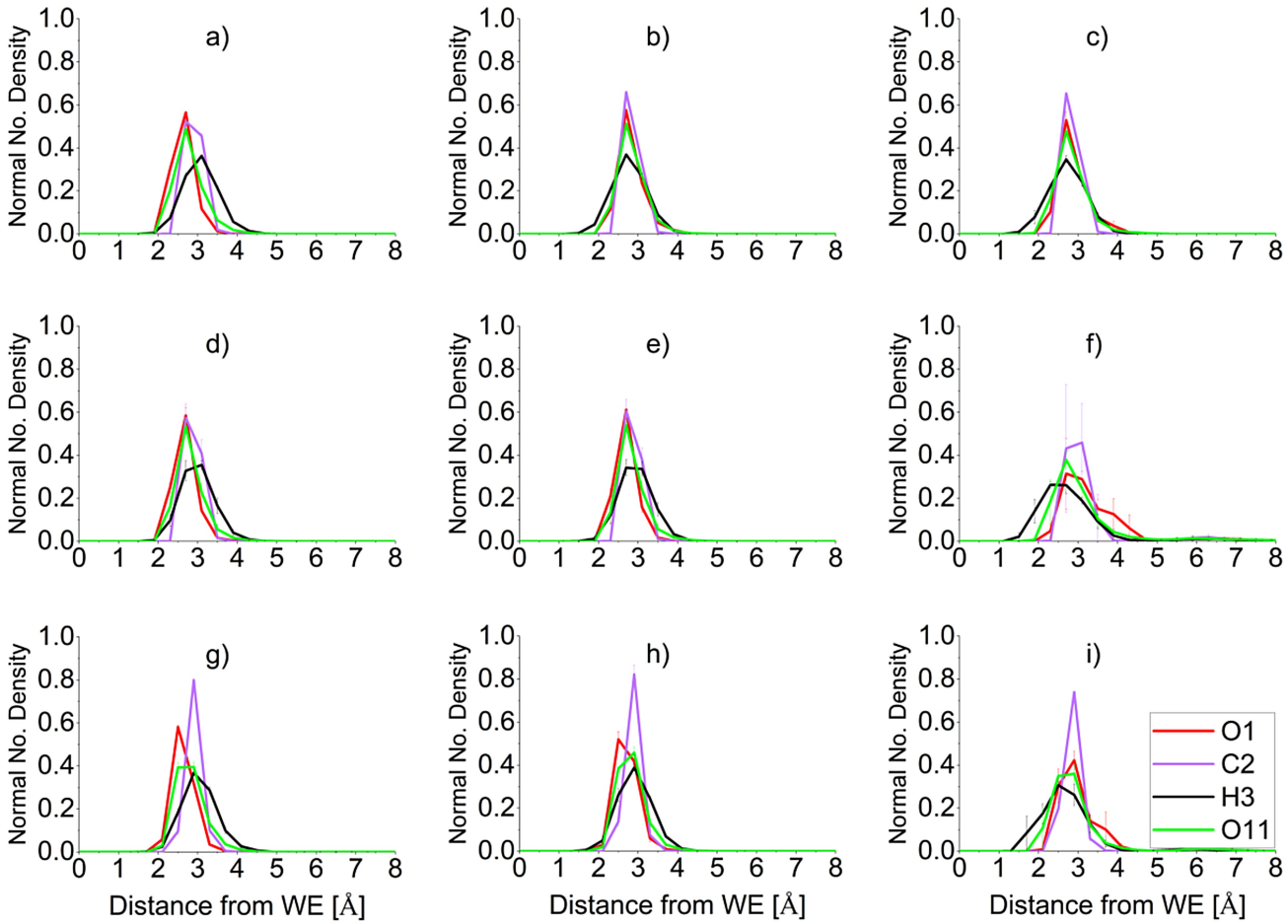

Figure 10. Density profile of different atoms of FF molecules (normalised with respect to the average number of adsorbed molecules on the working electrode (WE)) in Cu system versus distance to the WE for aqueous solution in a) 0 V, b) 1.5 V, c) 3.5 V cell voltage, for H_2SO_4 solution in d) 0 V, e) 1.5 V, f) 3.5 V cell voltage, and for HCl solution in g) 0 V, h) 1.5 V, i) 3.5 V cell voltage. O1, C2, H3 are atoms in the aldehyde group, and O11 is the oxygen in the furan ring.

interface layer. Therefore, the anions at the same time interact with the C2 and H3 atoms of FF with positive charges. However, the smaller chloride size might facilitate the movement and positioning of the anion to stay closer to the C2 and H3. Consequently, the C2 and H3 absorbed more the chloride while the O1 atoms absorbed at closer distance to the WE. On the other hand, the larger size of sulfate ions may prevent them to approach easily to the C2 and H3 atoms. However, at 1.5 V applied cell voltage in both aqueous (Figure 10b) and H_2SO_4 (Figure 10e) systems, the peaks for all visualized atoms occur at the same distance from WE. Again, in the HCl system at 1.5 V (Figure 10h), a higher tendency for O1 in the carbonyl group can be seen to adsorb on the surface. When we move to the 3.5 V simulations, for aqueous systems (Figure 10c), the highest number density for all atoms occurs at the same distance. However, in both acidic systems (H_2SO_4 and HCl), a wider distribution of atoms on WE can be seen in Figure 10f and i.

For all silver systems (in Figure 11) it can be observed that in contrast to the Cu system the peaks in the density profiles of the different atoms are widely distributed. This behaviour indicates the discrepancy between adsorption configurations of FF molecules on the silver electrode, i.e. the more tilted orientation of FF in contrast to the nearly parallel orientation in the Cu systems (Figure 8). The increasing uncertainties by increasing the applied voltages can also be seen in these figures, which can be explained by the higher dynamics of adsorbed molecules in the interface layer in these Ag systems. This attitude might be caused by the lower binding energy and lower interaction of FF molecules to the silver electrode.

In all simulated systems, it can be seen that by increasing the applied potential difference, the H3 curves approach more to the working electrode, which is the expected behavior due to the higher negative charges on the surface.

Hydrogen Bonding Analysis

A further insight into the interaction between solute and solvent in the hydrogenation process can be provided by computation of the Radial Distribution Function (RDF) and analysis of existence and lifetime of Hydrogen Bonding (HB) in the system. Availability and preservation of hydrogen bonding can influence the reaction process by affecting the hydration reaction. RDF shows the densities of one type of atoms or

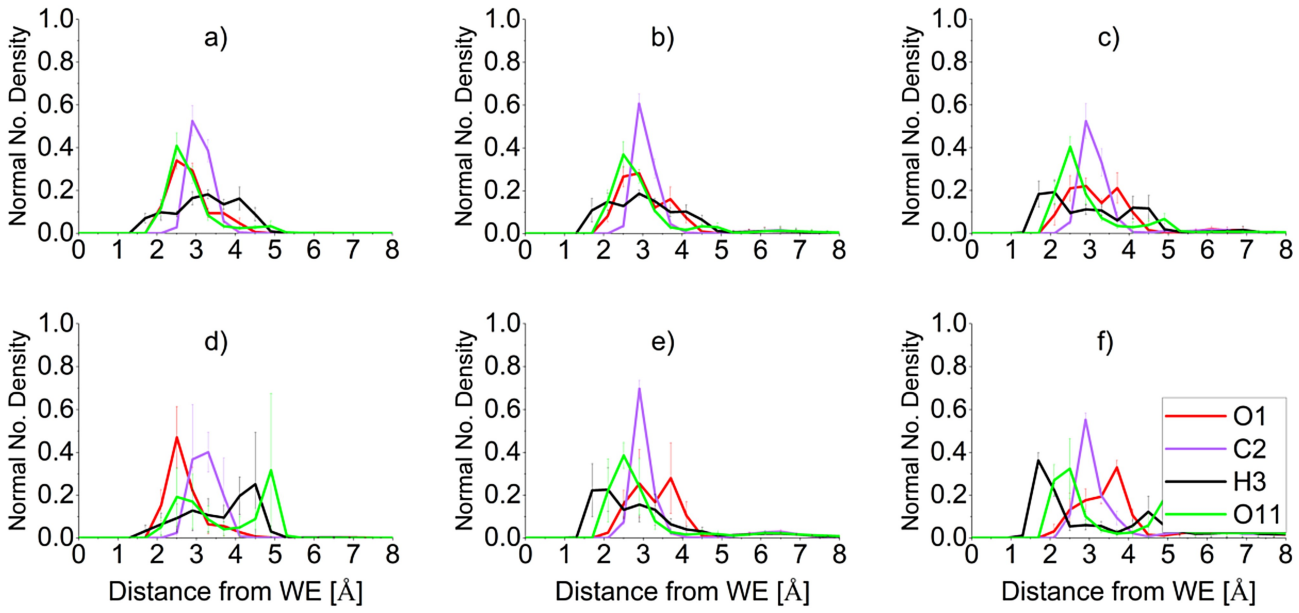

Figure 11. Density profile of different atoms of FF molecules (normalised with respect to the average number of adsorbed molecules on the working electrode (WE)) in Ag system versus distance to the WE for aqueous solution in a) 0 V, b) 1.5 V, c) 3.5 V cell voltage, and for H_2SO_4 solution in d) 0 V, e) 1.5 V, f) 3.5 V cell voltage. O1, C2, H3 are atoms in the aldehyde group, and O11 is the oxygen in the furan ring.

molecules as a distance to a reference particle. RDF among various atoms, provide basic information on the local organization of different moieties in the vicinity of each other. Due to the molecular structural of FF, it involves in a hydrogen bond as an acceptor of proton.[70,71] Therefore, RDFs were calculated between oxygen atoms in FF molecules and hydronium ions and water molecules to analyse the tendency for HB in the simulated systems. Among these pairs, we identified the interaction of water (Hw atom) and the hydronium ions (Hh atoms) with the oxygen in the aldehyde group (O1) of FF molecules as most relevant (SI, Figure S7–S11). Thus, the formation of HB was analysed by calculating the combined distribution function (CDF) between these two pairs (i.e. O1-Hw and O1-Hh). Figure 12 and Figure 13 depict exemplary CDF for O1-Hw and O1-Hh pairs in Ag and Cu system with H_2SO_4 solution at 0 V applied potential. In these figures, the x-axis

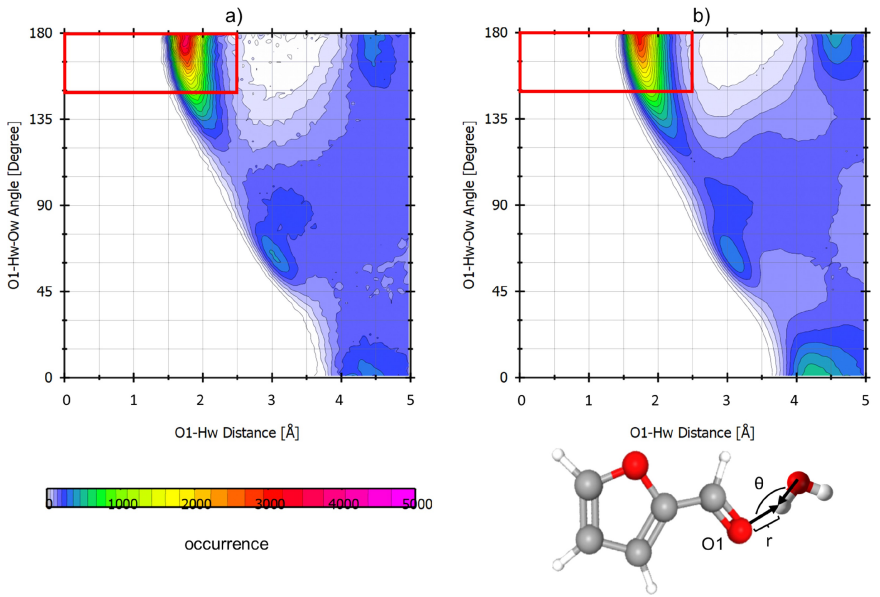

Figure 12. Combined distribution function (CDF) showing distance between the oxygen in the aldehyde group (O1) and hydrogen atom Hw of water molecules versus the angle between O1, Hw and Ow (oxygen of water molecules). The CDF illustrated for the FF system with H_2SO_4 at 0 V at a) Cu and b) Ag electrode. The red box shows a geometric criterion for a possible hydrogen bond.

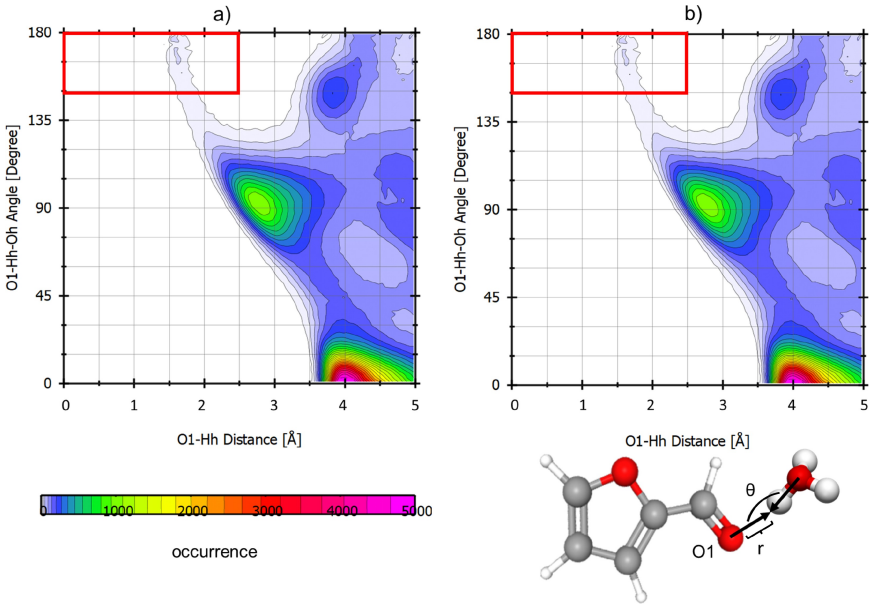

Figure 13. Combined distribution function (CDF) showing distance between the oxygen in the aldehyde group (O1) and hydrogen atom Hh of hydronium molecules versus the angle between O1, Hh and Oh (oxygen of hydronium ions). The CDF illustrated for the FF system with H_2SO_4 at 0 V at a) Cu and b) Ag electrode. The red box shows a geometric criterion for a possible hydrogen bond.

shows the distance between O1 and hydrogen in water (Hw) or hydrogen in hydronium ion (Hh), and the y-axis represents the angle between O1 and Hw–Ow bond in water or Hh–Oh bond in hydronium ion.

The HB was defined via geometric criteria with the distance of max. 2.5 Å between hydrogen donor X and acceptor Y and X–H···Y angle of 150°–180°,[72–74] as illustrated with a red box in Figure 12 and Figure 13. In Figure 12 can be seen, a high occurrence area is available around 2 Å and angle between 150–180°. However, in Figure 13 for both depicted systems, a low occurrence region presents in 150–180° at distance up to 2.5 Å. Therefore, by applying the HB criteria, it can be deduced that only the O1-Hw pair forms strong hydrogen bonding. Thus, in the following discussion we will focus on a further analysis of this HB. Figure 14 therefore presents the RDF curve for the O1-Hw pair for the FF in aqueous systems, in H_2SO_4 and HCl solutions at various applied voltages. As can be seen in Figure 14, the first peaks of RDF curves between O1 and Hw occurs at 1.85 Å distance between this pair for all simulated systems. The value of the peaks are lower than 1.0 in all cases, which shows that the probability of finding water around the O1 is lower than the bulk density. This was also reported in Ref. [70] for the solution of FF in water. In all three RDF curves in Figure 14, there was no correlation found between the changing applied voltages and the intensity of RDF peaks. Moreover, no significant changes were seen by adding H_2SO_4 or HCl to the electrolyte.

The dynamics of hydrogen bonding was investigated by calculation of HB aggregation lifetime in the interface layer with the defined geometric criteria. The HB aggregation lifetime were calculated between O1 in FF molecule and Hw in water molecule, the pair that has shown the strongest hydrogen bonding, as discussed above. According to the 50 fs output interval for trajectories, the HB lifetime calculation should be categorized as an intermittent lifetime with 50 fs interval. Figure 15 shows the HB lifetime for O1-Hw pair for different simulated systems.

As shown in Figure 15, the lifetime of HB in silver systems is shorter than the similar system with the Cu electrode. This might be related to the adsorption configuration of FF in the Ag systems in comparison to Cu, and the higher dynamics of the systems (see section Potential Changes). However, changing the applied potential has no significant effect on the HB lifetime of O1-Hw. As can be seen, adding ions to the system strengthened the HB for both electrodes in comparison to aqueous solution. This difference can be explained by the tendency of non-polar FF molecules to keep their distance from ions in the systems, which force them to have more interaction with water molecules.

Conclusions

In this work the fundamental parameters for the electrochemical hydrogenation of FF on Cu and Ag surfaces were investigated. Spectroscopic experiments were complemented by MD simulations to provide a fundamental knowledge of the investigated reaction. The structural and dynamic characteristics of the electrochemical system were studied in order to deepen the understanding of the molecular processes.

It could be shown from *in operando* Raman experiments and PMF simulations that FF molecules interact with both Cu and Ag electrodes. This is a necessary condition to progress the reaction at the electrode surface by strong educt adsorption.

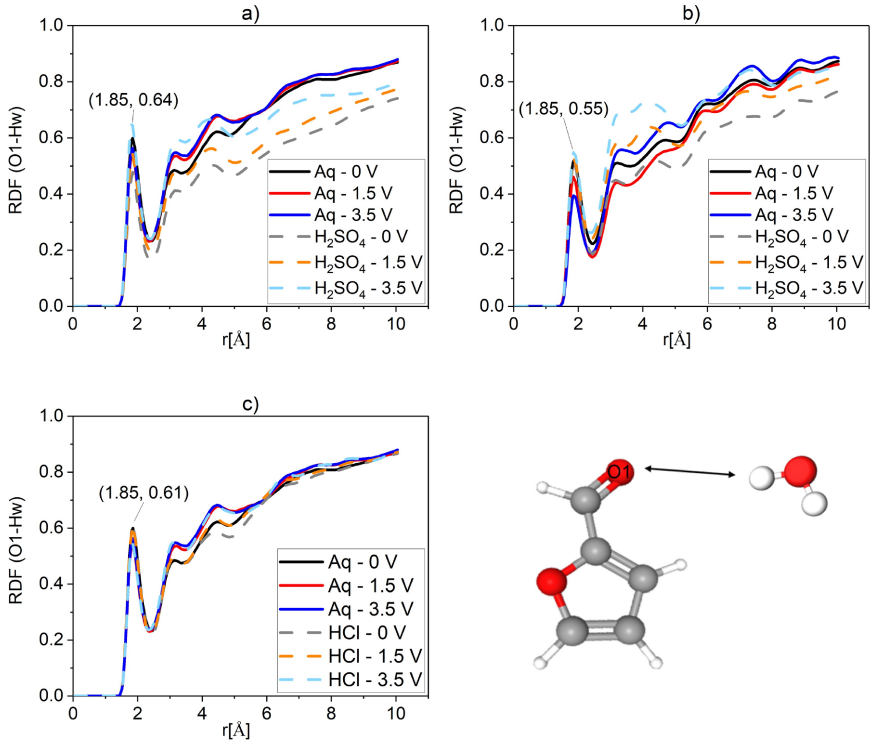

Figure 14. RDF curves between oxygen in aldehyde group (O1) and hydrogen of water moleules (Hw) for systems of 0.5 M FF in aqueous solution (Aq) and in H_2SO_4 solution with a) copper electrode, b) silver electrode and c) 0.5 M FF in HCl solution with copper electrode at various applied potential.

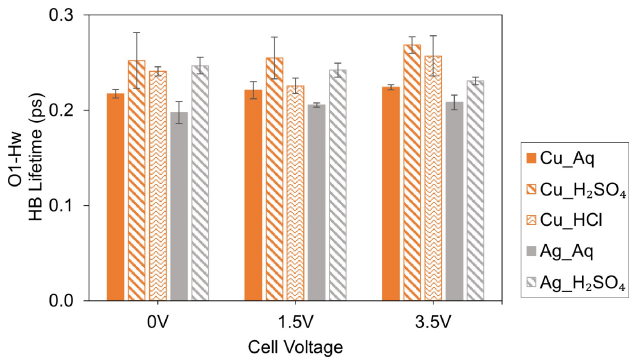

Figure 15. Hydrogen Bonding (HB) aggregation lifetime for O1 in FF molecules and Hw the hydrogen of water molecules at the copper and silver working electrode in different potential difference between electrodes (0 V, 1.5 V, 3.5 V) for Aq system, ionized sulfuric acid and ionized hydrochloric acid system.

Compared to Cu electrodes, Ag electrodes showed a weaker interaction with FF. Experimental results suggest that this behavior is enhanced with more negative potentials leading to a less efficient electrohydrogenation at Ag in comparison to Cu. While the aldehyde group interacts strongly with the metal surface, the furan ring also interacts with the metal surface for both metals. Both experiments and MD simulations results showed a parallel/slightly tilted orientation for Cu surface. Although on Ag surface the adsorption configuration of FF was more perpendicular than Cu, this configuration was still tilted and not completely perpendicular to the surface. Moreover, the preferable adsorption configuration of FF molecules at working electrode was illustrated and discussed by presenting the density profiles of different atoms in the FF molecules. The findings from this analysis showed the effect of changing electrode material and potential on adsorption configurations of FF molecules. Furthermore, potential and electrolyte concentrations relocated the equilibrium between *cis*- and *trans*-conformers.

Additionally, in experiments a lower contact time of FF molecules is observed with Ag electrode in comparison to Cu, and a higher dynamic in the Ag systems is also reflected in the MD simulations by higher uncertainties in the density profiles and shorter hydrogen bonding lifetime.

In addition, chloridic electrolytes were investigated. No significant changes in adsorption configuration of FF molecules were detected from MD simulations between chloride and sulfate anions. However, due to the poor signal-to-noise-ratio, no experimental adsorption configuration could be determined. The comparable weak signal intensity in the experimental results suggest a poorer interaction between metal and FF resulting in a higher distance to the surface. On the other side reaction performance parameters for FF hydrogenation in the literature showed only slightly poorer reaction performances. Discrepancies between these results require further investigations, e.g. in possible influences in SERS signal enhancement caused by different anion systems.

In the experiments, a change of the potential in a negative direction showed a product signal of FA/MF already at potentials, where macroscopically no product formation would be expected. While Cu exhibits an Cu–H formation already without applied potential, Ag develops an Ag–H signal at more negative potential. The relative signal intensity of both Cu–H and Ag–H signals increases with more negative potentials, indicating an increased amount of adsorbed hydrogen, enabling its possible function as electron carrier in the reaction mechanism.

The analysis of RDFs in the MD studies have shown that in all investigated systems, strong hydrogen bonding is formed between oxygen atom of FF in aldehyde group and water molecules, though with the lowest peaks observed in the Ag systems. For all systems, the HB lifetime increased by adding acid in the electrolyte.

Despite the applied simplifications in the MD models for conducting feasible simulations, the results were in agreement with the findings from the experiments. Moreover, the MD simulations provided complementary insight into the characteristics of the studied systems. Further investigations on the influence of selected metal facets and electrolyte composition could be useful for future works.

All in all, findings from this work provide a deep insight into the electrohydrogenation of FF and contribute in many ways to identifying the main determinants in this reaction process.

The data that support the findings of this study are available from the corresponding author upon reasonable request. The list of force field parameters, as well as an example input file for the GROMACS and LAMMPS simulations are provided in a github repository [https://github.com/saharrabet/ChemPhysChem2022].

Acknowledgements

We would like to acknowledge the funding by the Deutsche Forschungsgemeinschaft (DFG, German Research Foundation) under Germany's Excellence Strategie – EXC 2163-1 – Sustainable and Energy Efficient Aviation – Project ID 390881007. The authors also acknowledge support by the DFG Major Instrumentation Program (INST 188/420-1 FUGG). The MD simulations were carried out on a cluster of North-German Supercomputing Alliance (HLRN). The authors greatly appreciate the support. The authors would like to thank Prof. Gregory A. Voth and his group for providing the LAMMPS model for the simulation of polarizable electrode. Open Access funding enabled and organized by Projekt DEAL.

Conflict of Interest

The authors declare no conflict of interest.

Keywords: Electrochemical Synthesis · Electrofuel · Furfural · Molecular Dynamics · Raman Spectroscopy

[1] X. Li, P. Jia, T. Wang, *ACS Catal.* **2016**, *6*, 7621.
[2] C. H. Lam, W. Deng, L. Lang, X. Jin, X. Hu, Y. Wang, *Energy Fuels* **2020**, *34*, 7915. .
[3] T. Werpy, G. Petersen, Top Value Added Chemicals from Biomass Volume I – Results of Screening for Potential Candidates from Sugars and Synthesis Gas, Technical report, US Department of Energy, Washington DC **2004**.
[4] A. Goldmann, W. Sauter, M. Oettinger, T. Kluge, U. Schröder, J. R. Seume, J. Friedrichs, F. Dinkelacker, *Energies* **2018**, *11*, 392.
[5] P. Nilges, U. Schröder, *Energy Environ. Sci.* **2013**, *6*, 2925.
[6] S. Jung, E. J. Biddinger, *ACS Sustainable Chem. Eng.* **2016**, *4*, 6500.
[7] A. S. May, E. J. Biddinger, *ACS Catal.* **2020**, *10*, 3212.
[8] X. H. Chadderdon, D. J. Chadderdon, J. E. Matthiesen, Y. Qiu, J. M. Carraher, J. P. Tessonnier, W. Li, *J. Am. Chem. Soc.* **2017**, *139*, 14120.
[9] Y. Kwon, K. J. P. Schouten, J. C. Van Der Waal, E. De Jong, M. T. Koper, *ACS Catal.* **2016**, *6*, 6704.
[10] A. S. May, S. M. Watt, E. J. Biddinger, *React. Chem. Eng.* **2021**, *6*, 2075.
[11] F. Harnisch, U. Schröder, *ChemElectroChem* **2019**, *6*, 4126.
[12] D. Y. Wu, J. F. Li, B. Ren, Z. Q. Tian, *Chem. Soc. Rev.* **2008**, *37*, 1025.
[13] J. E. Pemberton, M. A. Bryant, R. L. Sobocinski, S. L. Joa, *J. Phys. Chem.* **1992**, *96*, 3776.
[14] A. Wang, Y. F. Huang, U. K. Sur, D. Y. Wu, B. Ren, S. Rondinini, C. Amatore, Z. Q. Tian, *J. Am. Chem. Soc.* **2010**, *132*, 9534.
[15] N. Heidary, N. Kornienko, *Chem. Commun.* **2019**, *55*, 11996.
[16] N. Heidary, N. Kornienko, *Chem. Sci.* **2020**, *11*, 1798.
[17] D. Ibañez, A. Santidrian, A. Heras, M. Kalbáč, A. Colina, *J. Phys. Chem. C* **2015**, *119*, 8191.
[18] J. Anibal, B. Xu, *ACS Catal.* **2020**, *10*, 11643.
[19] J. Li, N. Kornienko, *Chem. Commun.* **2021**, *57*, 5127.
[20] S. Wang, H. Dang, W. Xue, D. Shields, X. Liu, F. C. Jentoft, D. E. Resasco, *Int. J. Phys. Math. Sci.* **2013**, *7*, 1104.
[21] V. Vorotnikov, G. Mpourmpakis, D. G. Vlachos, *ACS Catal.* **2012**, *2*, 2496.
[22] Y. Shi, Y. Zhu, Y. Yang, Y.-W. Li, H. Jiao, *ACS Catal.* **2015**, *5*, 4020.
[23] Z. Zhao, R. Bababrik, W. Xue, Y. Li, N. M. Briggs, D.-T. Nguyen, U. Nguyen, S. P. Crossley, S. Wang, B. Wang, et al., *Nat. Catal.* **2019**, *2*, 431.
[24] L. Scalfi, M. Salanne, B. Rotenberg, *Annu. Rev. Phys. Chem.* **2021**, *72*, 189, pMID: 33395545.
[25] J.-B. Le, X.-H. Yang, Y.-B. Zhuang, M. Jia, J. Cheng, *J. Phys. Chem. Lett.* **2021**, *12*, 8924.
[26] M. K. Petersen, R. Kumar, H. S. White, G. A. Voth, *J. Phys. Chem. C* **2012**, *116*, 4903.
[27] J. I. Siepmann, M. Sprik, *J. Chem. Phys.* **1998**, *102*, 511.
[28] S. K. Reed, P. A. Madden, A. Papadopoulos, *J. Chem. Phys.* **2008**, *128*, 124701.
[29] P. Gao, D. Gosztola, L. W. H. Leung, M. J. Weaver, *J. Electroanal. Chem.* **1987**, *233*, 211.
[30] T. Kim, R. S. Assary, L. A. Curtiss, C. L. Marshall, P. C. Stair, *J. Raman Spectrosc.* **2011**, *42*, 2069.
[31] E. Sobolev, V. Aleksanyan, R. Karakhanov, I. Bel'skii, V. Ovodova, *Commision on Spectroscopy, Academy of Science* **1963**, *4*, 358.
[32] S. Plimpton, *J. Comput. Phys.* **1995**, *117*, 1.
[33] M. J. Abraham, T. Murtola, R. Schulz, S. Páll, J. C. Smith, B. Hess, E. Lindahl, *SoftwareX* **2015**, *1–2*, 19.
[34] W. L. Jorgensen, J. Tirado-Rives, *J. Am. Chem. Soc.* **1988**, *110*, 1657, pMID: 27557051.
[35] S. Rabet, G. Raabe, *Fluid Phase Equilib.* **2022**, *554*, 113331.
[36] S. Halstead, P. An, S. Zhang, *Mol. Phys.* **2014**, *112*, 2235.
[37] W. L. Jorgensen, J. Chandrasekhar, J. D. Madura, R. W. Impey, M. L. Klein, *J. Chem. Phys.* **1983**, *79*, 926.
[38] M. G. Wolf, G. Groenhof, *J. Comput. Chem.* **2014**, *35*, 657.
[39] H. Heinz, R. Vaia, B. Farmer, R. Naik, *J. Phys. Chem. C* **2008**, *112*, 17281.
[40] L. Martínez, R. Andrade, E. G. Birgin, J. M. Martínez, *J. Comput. Chem.* **2009**, *30*, 2157.
[41] A. Mecklenfeld, G. Raabe, *J. Chem. Theory Comput.* **2017**, *13*, 6266.
[42] T. Darden, D. York, L. Pedersen, *J. Chem. Phys.* **1993**, *98*, 10089.
[43] S. Miyamoto, P. A. Kollman, *J. Comput. Chem.* **1992**, *13*, 952.
[44] G. M. Torrie, J. P. Valleau, *J. Comput. Phys.* **1977**, *23*, 187.
[45] J. Kästner, *Wiley Interdiscip. Rev.: Comput. Mol. Sci.* **2011**, *1*, 932.
[46] S. Kumar, J. M. Rosenberg, D. Bouzida, R. H. Swendsen, P. A. Kollman, *J. Comput. Chem.* **1992**, *13*, 1011.
[47] J. S. Hub, B. L. De Groot, D. Van Der Spoel, *J. Chem. Theory Comput.* **2010**, *6*, 3713.
[48] S. Nosé, *J. Chem. Phys.* **1984**, *81*, 511.
[49] W. G. Hoover, *Phys. Rev. A* **1985**, *31*, 1695.
[50] J.-P. Ryckaert, G. Ciccotti, H. J. Berendsen, *J. Comput. Phys.* **1977**, *23*, 327.

[51] Hockney, Eastwood, *Adam Hilger, NY* **1989**.
[52] A. Stukowski, *Model. Simul. Mater. Sci. Eng.* **2009**, *18*, 015012.
[53] W. Humphrey, A. Dalke, K. Schulten, *J. Mol. Graphics* **1996**, *14*, 33.
[54] M. Brehm, B. Kirchner, *J. Chem. Inf. Model.* **2011**, *51*, 2007.
[55] M. Brehm, M. Thomas, S. Gehrke, B. Kirchner, *J. Chem. Phys.* **2020**, *152*, 164105.
[56] T.-j. Jia, P.-w. Li, Z.-g. Shang, L. Zhang, T.-c. He, Y.-j. Mo, *J. Mol. Struct.* **2008**, *873*, 1.
[57] Y. Fleger, Y. Mastai, M. Rosenbluh, D. Dressler, *J. Raman Spectrosc.* **2009**, *40*, 1572.
[58] K. Bunding, M. Bell, *Surf. Sci.* **1982**, *118*, 329.
[59] Y. Chen, Z. Tian, *Chem. Phys. Lett.* **1997**, *281*, 379.
[60] X. Gao, J. P. Davies, M. J. Weaver, *J. Phys. Chem.* **1990**, *94*, 6858.
[61] G. Schultz, I. Fellegvári, M. Kolonits, A. Kiss, *J. Mol. Struct.* **1978**, *50*, 325.
[62] M. Rogojerov, G. Keresztury, B. Jordanov, *Spectrochim. Acta Part A* **2005**, *61*, 1661.
[63] B. Liu, L. Cheng, L. Curtiss, J. Greeley, *Surf. Sci.* **2014**, *622*, 51.
[64] Z.-Q. Tian, B. Ren, *Annu. Rev. Phys. Chem.* **2004**, *55*, 197.
[65] Z. Q. Tian, B. Ren, Y. X. Chen, S. Z. Zou, B. W. Mao, *J. Chem. Soc. Faraday Trans.* **1996**, *92*, 3829.
[66] N. Shan, M. K. Hanchett, B. Liu, *J. Phys. Chem. C* **2017**, *121*, 25768.
[67] J. J. Roylance, T. W. Kim, K. S. Choi, *ACS Catal.* **2016**, *6*, 1840.
[68] N. Leopold, A. Stefancu, K. Herman, I. S. Tódor, S. D. Iancu, V. Moisoiu, L. F. Leopold, *Beilstein J. Nanotechnol.* **2018**, *9*, 2236.
[69] D. Markthaler, S. Jakobtorweihen, N. Hansen, *Living J. Comp. Mol. Sci.* **2019**, *1*, 11073.
[70] F. Grote, I. Ermilova, A. P. Lyubartsev, *J. Phys. Chem. B* **2018**, *122*, 8416.
[71] R. Rivelino, S. Canuto, K. Coutinho, *Braz. J. Phys.* **2004**, *34*, 84.
[72] J. Emsley, *Chem. Soc. Rev.* **1980**, *9*, 91.
[73] G. A. Jeffrey, W. Saenger, *Hydrogen bonding in biological structures*, Springer Science & Business Media **2012**.
[74] Y. Maréchal, The hydrogen bond and the water molecule: The physics and chemistry of water, aqueous and bio-media, Elsevier **2006**.

Manuscript received: August 17, 2022
Revised manuscript received: October 31, 2022
Accepted manuscript online: November 7, 2022
Version of record online: December 5, 2022